The Reduction of Force Component Produced by Short Sides by Analyzing the Corner of Coil in Planar Motor with Halbach Magnet Array

Guangdou Liu, Shiqin Hou, and Wensheng Xiao*

College of Mechanical and Electronic Engineering
China University of Petroleum, Qingdao 266580, China
gdliu@upc.edu.cn, 1334273282@qq.com, xiaows@upc.edu.cn*

Abstract ─ The planar motor with moving-magnet is purely levitated by the stator coils. The forces produced by coils are calculated with the analytical model of magnet array and coil surface model for applying to the real time control. Take the coil and the Halbach magnet array which is at 45 degree with the long side of coil for analysis. The force component produced by short sides can be eliminated for conveniently controlling when the length of coil takes certain dimension. In practice, the force component produced by short sides is small but not zero. There are two reasons, one is the higher harmonics and the other is the corner segments of coil. The force integral expressions of coil corner segments are given by the Lorenz force law. Then the forces numerically calculated with harmonic model and coil full model are verified by comparing with the magnetic surface charge model and finite element model. In order to reduce the force component produced by short sides, the different corners of coil are analyzed. Comparing the forces of different corners of coil, the force component produced by short sides can be significantly reduced with slightly change of the other force components.

Index Terms ─ Corner segments, force reduction, Halbach array, planar motor.

I. INTRODUCTION

The magnetically levitated planar motor with moving magnets is attracting more and more attention with the advantages of high speed, high acceleration and high precision in the industry. The moving magnet array is purely levitated by the suspension force exerted by coils, and realizes the horizontal motion [1-13]. There are no transmission equipment, so the planar motor is without the mechanical friction, lubricating oil contamination, cable interference and so on. The structure of the planar motor is simplified, and of which the weight is reduced. The 2D Halbach permanent magnet array is applied in the planar motor, which can obtain high magnetic field on one side with fine sinusoidal waveform [6].

Compter [7] proposed the magnetically levitated planar motor with moving coils, and the magnet array is rotated -45° relative to the coils. The planar motor replaces the conventional structure with two linear motors to realize the horizontal motion. Jansen [8] applied the arrangement of coil and the magnet array to the planar motor of moving magnets, which is the inverse of planar motor of moving coils. The harmonic model of magnetic flux density for the Halbach magnet array is derived by Fourier series and scalar potential. The forces and torques generated by coils are calculated by using analytical model which is obtained by taking the first harmonic and coil surface model in order to be used in the real time control. Jansen [9] optimized the planar motor with moving magnets. The minimum power dissipation at the suspension status is selected to be the optimized objective function. The optimal dimensions of coil and magnet array are obtained. Peng [10] took the coil corner segments into account for calculating the force and torque of coil. The expressions of force and torque are derived by using the composite integration and the Newton-Leibniz formula with the analytical model of magnet array. But the higher harmonics is ignored.

As the Halbach magnet array is at 45 degree with the long side of one coil, the force component produced by short sides of coil can be eliminated when the length of coil takes certain dimension according to the force expression used in the real time control. In fact, the force is not zero due to the higher harmonics and corner segments of coil. In this paper, the integral force expression for the corner segments of coil is derived by the Lorenz force law. The forces calculated by using harmonic model and coil full model are verified to be accurate. The different winding moulds are proposed and the different coil structures are obtained. The forces of different coils are predicted by using the model verified before. Comparing the forces of different coils, the component produced by short sides can be

significantly reduced with slightly change of the other force components.
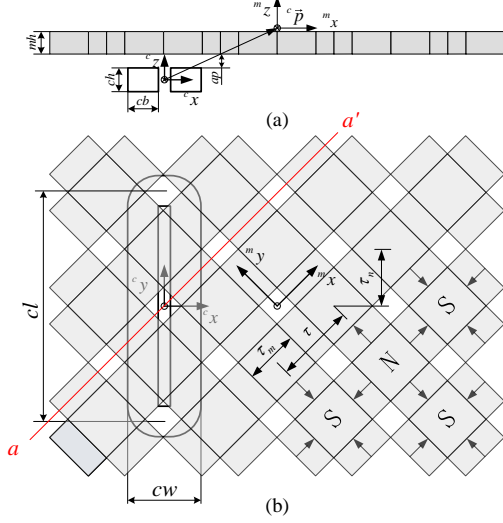
Fig. 1. The sketch of one coil and the Halbach magnet array in planar motor: (a) front view and (b) top view.

II. THE PLANAR MOTOR

The sketch of one coil and the Halbach magnet array in planar motor with moving magnets is shown in Fig. 1. In Fig. 1, the arrows mean the magnetization direction of magnets from s-pole to n-pole. N shows the magnetization direction outward the paper which is consistent with the positive direction of $^m z$ axis, and S is in the opposite direction. The global and local coordinates are located at the center of the coils and the Halbach magnet array, which are denoted with the superscript ^{c} and ^{m}, respectively.

The magnetic flux density of the Halbach magnet array shown in Fig. 1 is spatial distribution. The magnetic flux density is derived by using Fourier series and scalar potential and expressed in the local coordinate system. The derivation procedure is shown in reference [11]. The expression is:

$$^m\vec{B}_3\left(^m\vec{x}\right) = -\mu_0 \cdot$$

$$\sum_{m=1}^{\infty}\sum_{n=1}^{\infty} K_3 e^{\lambda\,^m z} \begin{bmatrix} \dfrac{k\pi}{\tau}\cos\dfrac{k\pi\,^m x}{\tau}\sin\dfrac{l\pi\,^m y}{\tau} \\[2mm] \dfrac{l\pi}{\tau}\sin\dfrac{k\pi\,^m x}{\tau}\cos\dfrac{l\pi\,^m y}{\tau} \\[2mm] \lambda\sin\dfrac{k\pi\,^m x}{\tau}\sin\dfrac{l\pi\,^m y}{\tau} \end{bmatrix}, \quad (1)$$

where $\mu_r = 1$, and

$$\lambda = \frac{\pi}{\tau}\sqrt{k^2 + l^2}, \quad (2)$$

$$a(k) = \frac{4}{k\pi}\cos\frac{k\tau_m\pi}{2\tau}\sin\frac{k\pi}{2}, \quad (3)$$

$$b(k) = \frac{4}{k\pi}\sin\frac{k\tau_m\pi}{2\tau}\sin\frac{k\pi}{2}, \quad (4)$$

$$K_3 = B_r\frac{\left(e^{-m_t\lambda} - e^{-m_b\lambda}\right)}{2\left(k^2 + l^2\right)\pi\lambda\mu_0}\begin{pmatrix} b(k)b(l)\pi\left(k^2 + l^2\right) \\ +a(k)b(l)k\lambda\tau \\ +a(l)b(k)l\lambda\tau \end{pmatrix}, \quad (5)$$

k and l are the harmonic numbers for the $^c x$- and $^c y$-direction, respectively, m_t and m_b are the height of magnet array, τ_m is the side length of the magnets magnetized in the $^c z$-direction, τ is the pole pitch, B_r is the residual magnetization of the permanent magnet, μ_r is the relative permeability of the permanent magnets, μ_0 is the permeability of vacuum.

Because the high quality sintered NdFeB permanent magnets ($\mu_r \approx 1.03\text{-}1.05$) is used in the planar motor. The relative permeability of the permanent magnets is considered equal to air, the error due to this assumption can be neglected.

The coil shown in Fig. 1 can be split into eight segments, including four straight segments and four corner segments. The Lorenz force law is applied to the calculation of force produced by coil [12]. The force expression is:

$$\begin{aligned} ^c\vec{F} &= -\int_{Vcoil} \vec{j} \times\, ^c\vec{B}_3\, d\,^c V \\ &= -\left(\int_{Vstraight}\vec{j}\times\,^c\vec{B}_3\,d\,^c V + \int_{Vcorner}\vec{j}\times\,^c\vec{B}_3\,d\,^c V\right), \end{aligned} \quad (6)$$

The force F_y produced by short sides of coil shown in Fig. 1 is analyzed. In order to satisfied the real time control, the coil surface model and analytical model of Halbach magnet array are used [5]. The force F_y can be expressed as:

$$^c F_y = -jB_z e^{-\frac{\sqrt{2}\pi}{\tau}\,^c p_z}\left(cw - cb\right)\left(\frac{\tau}{\pi}\right)^2$$
$$\sin\frac{cb\sqrt{2}\pi}{2\tau}\sin\frac{cl\sqrt{2}\pi}{2\tau}\sin\frac{\left(^c y - \,^c p_y\right)\sqrt{2}\pi}{\tau}, \quad (7)$$

where

$$B_z = \sqrt{2}K_3\frac{\pi}{\tau}, \quad (8)$$

j is the surface current of coil, $^c p_z$ and $^c p_y$ are the coordinate of the point $^c\vec{p}$ shown in Fig. 1, cb is the conductor bundle width, cl is the length of coil.

The force F_y can be eliminated when $cl = \sqrt{2}n\tau$. Due to the higher harmonics and corner segments of coil, the actual force F_y is not zero.

The method of changing the structure of coil to reduce the force F_y is proposed. The different coils are obtained by changing the winding mould. The forces of these coils are predicted by using harmonic model and coil full model.
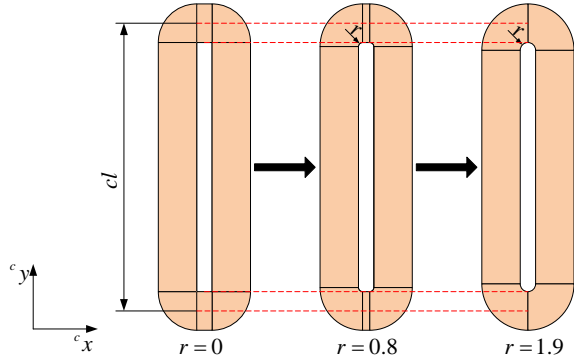
Fig. 2. The different corners of coil with different winding moulds.

III. COILS AND FORCE EXPRESSIONS

The different winding moulds are obtained by filleting the four edges. The different coils are shown in Fig. 2. The coil length cl keeps constant of these coils.

The dimensions of coil and magnets are decided according to the reference [6], and are listed in the Table 1 shown as follows.

Table 1: The dimensions of coil and magnets

Parameters	Value	Unit
Pole pitch (τ)	25	mm
Pole pitch of coordinate transformation (τ_n)	17.7	mm
Magnet pitch (τ_m)	17	mm
Clearance (ap)	1	mm
Coil length (cl)	70.8	mm
Coil width (cw)	22.8	mm
Conductor bundle width (cb)	9.5	mm
Coil height (ch)	7.4	mm
Remanence of the magnet (B_r)	1.24	T
current density (j)	10	A/mm²
Magnet array height (mh)	7	mm

Take the coil with r=0.8mm for example to derive the force expressions of corner segments of coil. Figure 3 shows the coil, and there are eight segments marked with number from 1 to 8.
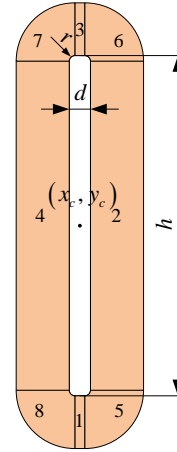
Fig. 3. The segments and dimensions of coil.

A. The straight segments of coil

The force expression of straight segments can be directly given by the Lorenz force law,

$$
{}^{c}\vec{F}_{straight} =
$$

$$
-\int_{z_1}^{z_2}\int_{y_c-\frac{h}{2}-cb}^{y_c-\frac{h}{2}}\int_{x_c-\frac{d}{2}+r}^{x_c+\frac{d}{2}-r}\begin{bmatrix} j & 0 & 0 \end{bmatrix}^{\mathrm{T}} \times {}^{c}\vec{B}_3\, d\,{}^{c}x\, d\,{}^{c}y\, d\,{}^{c}z
$$

$$
-\int_{z_1}^{z_2}\int_{y_c-\frac{h}{2}+r}^{y_c+\frac{h}{2}-r}\int_{x_c+\frac{d}{2}}^{x_c+\frac{d}{2}+cb}\begin{bmatrix} 0 & j & 0 \end{bmatrix}^{\mathrm{T}} \times {}^{c}\vec{B}_3\, d\,{}^{c}x\, d\,{}^{c}y\, d\,{}^{c}z \quad , (9)
$$

$$
-\int_{z_1}^{z_2}\int_{y_c+\frac{h}{2}}^{y_c+\frac{h}{2}+cb}\int_{x_c-\frac{d}{2}+r}^{x_c+\frac{d}{2}-r}\begin{bmatrix} -j & 0 & 0 \end{bmatrix}^{\mathrm{T}} \times {}^{c}\vec{B}_3\, d\,{}^{c}x\, d\,{}^{c}y\, d\,{}^{c}z
$$

$$
-\int_{z_1}^{z_2}\int_{y_c-\frac{h}{2}+r}^{y_c+\frac{h}{2}-r}\int_{x_c-\frac{d}{2}-cb}^{x_c-\frac{d}{2}}\begin{bmatrix} 0 & -j & 0 \end{bmatrix}^{\mathrm{T}} \times {}^{c}\vec{B}_3\, d\,{}^{c}x\, d\,{}^{c}y\, d\,{}^{c}z
$$

where

$$
z_1 = -mh - ap - ch , \tag{10}
$$

$$
z_2 = -mh - ap , \tag{11}
$$

${}^{c}\vec{B}_3$ is the transformation of the ${}^{m}\vec{B}_3$ into the global coordinate system, x_c, y_c are the coordinate value of the geometric center of coil in the global coordinate system, d and h are the length and width of the winding mould, respectively, r is the fillet radius.

B. The corner segments of coil

The corner segment 5 is picked for analyzing. There are two parts to be analyzed for calculating the force, the big circle and the small circle. The small circle segment will be subtracted in the force calculation. The current is in counter-clockwise direction.

The direction of current in the corner segment at any point is the tangential direction shown in Fig. 4, which can be decomposed into x- and y-component.

The two components are denoted with j_{5x} and j_{5y}, respectively. The expressions of j_{5x} and j_{5y} are described by:

$$j_{5x} = -j \frac{{}^c y - y_5}{\sqrt{\left({}^c x - x_5\right)^2 + \left({}^c y - y_5\right)^2}}, \quad (12)$$

$$j_{5y} = j \frac{{}^c x - x_5}{\sqrt{\left({}^c x - x_5\right)^2 + \left({}^c y - y_5\right)^2}}, \quad (13)$$

where

$$x_5 = x_c + \frac{d}{2} - r, \quad (14)$$

$$y_5 = y_c - \frac{h}{2} + r, \quad (15)$$

x_5 and y_5 are the coordinate value of the center point of the circle.
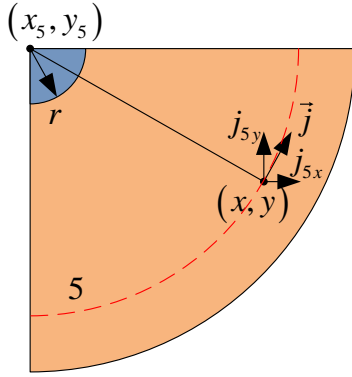
Fig. 4. The corner segment 5 of coil.

The force expression of the big circle segment is given by:

$$ {}^c\vec{F}_{51} = -\int_{z_1}^{z_2} \int_{x_c+\frac{d}{2}-r}^{x_c+\frac{d}{2}+cb} \int_{f_{51}({}^c x)}^{y_c-\frac{h}{2}+r} \cdot \\ \left[j_{5x} \quad j_{5y} \quad 0 \right]^{\mathrm{T}} \times {}^c\vec{B}_3 d^c x d^c y d^c z $$

$$(16)$$

where

$$f_{51}({}^c x) = -\sqrt{(cb+r)^2 - (x - x_{51})^2} + y_{52}, \quad (17)$$

The current expressions in the small circle are the same as the big circle segment. The force expression can be expressed as:

$$ {}^c\vec{F}_{52} = -\int_{z_1}^{z_2} \int_{x_c+\frac{d}{2}-r}^{{}^c x+\frac{d}{2}} \int_{f_{52}({}^c x)}^{y_c-\frac{h}{2}+r} \cdot \\ \left[j_{5x} \quad j_{5y} \quad 0 \right]^{\mathrm{T}} \times {}^c\vec{B}_3 d^c x d^c y d^c z $$

$$(18)$$

where

$$f_{52}({}^c x) = -\sqrt{r^2 - (x - x_{51})^2} + y_{52}, \quad (19)$$

Finally, the force expression of the corner segment 5 of coil is obtained and is expressed as:

$$ {}^c\vec{F}_5 = {}^c\vec{F}_{51} - {}^c\vec{F}_{52}, \quad (20) $$

The force expression of the other corner segments can be obtained by using the same method.

The force of the coil is calculated by using the harmonic model and coil full model, and the center point ${}^c\vec{p}$ of Halbach magnet array is along the line $a - a'$. In order to verify the accuracy, the forces calculated with harmonic model, magnetic surface charge model and finite element model are compared. The finite element model is obtained by the Ansoft Maxwell with percent error 0.1, which is a very professional electromagnetic field analysis software. The F_x and F_z of three models are shown in Fig. 5.
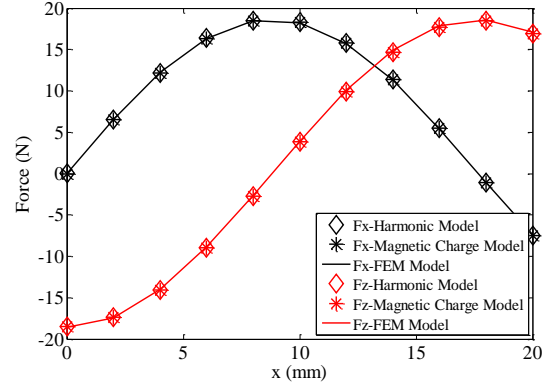
Fig. 5. The comparison of F_x and F_z of three models.

From the Fig. 5, it is found the error between the harmonic model and magnetic surface charge model is very small. Both the two models keep good consistency with the finite element model. For the F_z, the max error between the harmonic model and magnetic surface charge model is 0.032N and 0.203N between the harmonic model and finite element model, which are the 0.2% and 1.28% of the peak value of the harmonic, respectively.
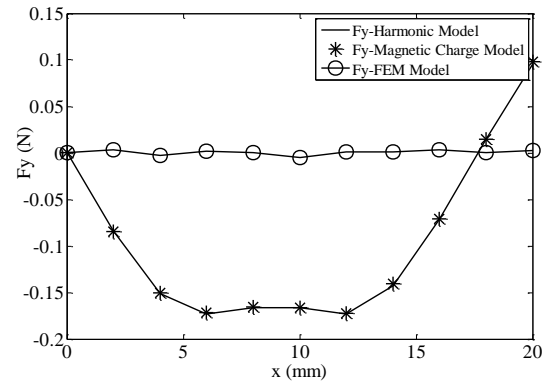
Fig. 6. The comparison of F_y of three models.

Figure 6 shows the F_y of three models. The force

F_y is small but not zero. The forces F_y of the harmonic model and magnetic surface charge model are in good agreement. The finite element model is not correct due to the small force F_y and the max error 0.203N obtained by F_z. The harmonic model is verified and selected to predict the force of different coils.

IV. FORCES OF DIFFERENT COILS

The different coils are obtained when fillet radius r takes 0, 0.5, 0.8, 1.2, 1.6 and 1.9. The forces are calculated and compared among these coils.

Figure 7 shows the comparison of F_x of different coils. The F_x decreases with the fillet radius r increase. The error of the peak value between the coil with r=0 and the coil with r=1.9 is 0.318N. It is the 1.70% of the peak value of the coil with r=0. The change of F_x is samll from the comparison.
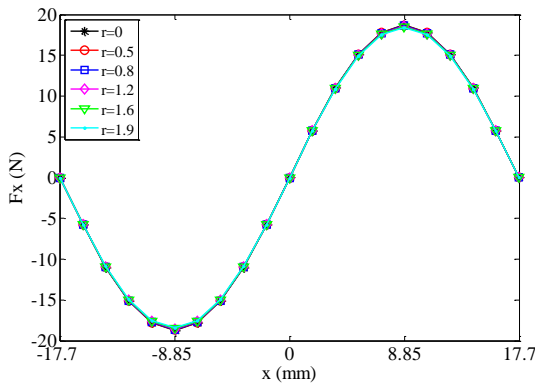
Fig. 7. The comparison of F_x of three models.
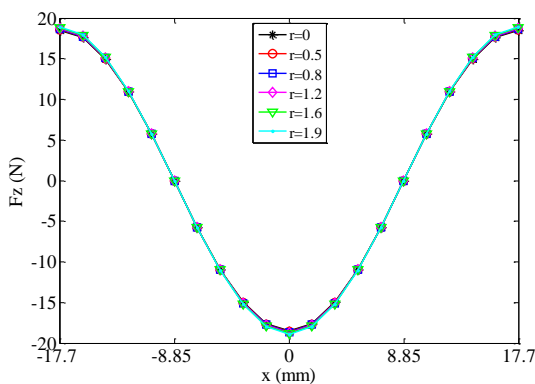
Fig. 8. The comparison of F_z of three models.

Figure 8 shows the comparison of F_z of different coils. The F_z increases with the increasing fillet radius r. The error of the peak value between the coil with r=0 and the coil with r=1.9 is 0.388N. It is the 2.10% of the

peak value of the coil with r=0. The change of F_z is samll from the comparison.

Figure 9 shows the comparison of F_y of different coils. It is found that the F_y decreases firstly to zero and then increases reversely with the fillet radius increase. In order to distinguish the forces generated by straight segments from the corner segments of coil, the F_y of two parts are compared.

The straight segments 1 and 3 of coil produce the force F_y. The range of straight segments 1 and 3 decreases with the fillet radius increase, so does the force F_y. Figure 10 shows the F_y generated by straight segments of these coils, which is in accordance with the inference. The magnitude of the F_y of the straight segment is very small.
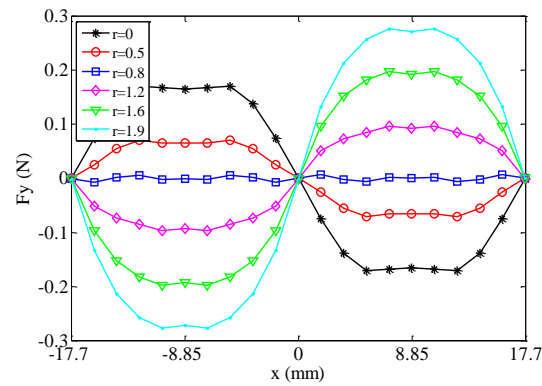
Fig. 9. The comparison of F_y of different coils.
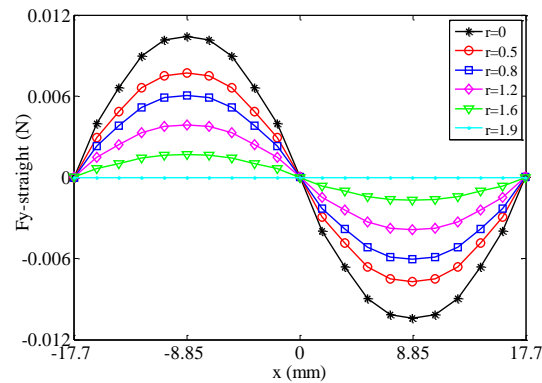
Fig. 10. The comparison of F_y generated by straight segments of different coils.

The major component of F_y is generated by corner segments of coil. To be more comprehensive, the F_y with different fillet radius are compared in one period, and is shown in the Fig. 11. The maximum value of F_y for each coil is listed in the Table. 2.
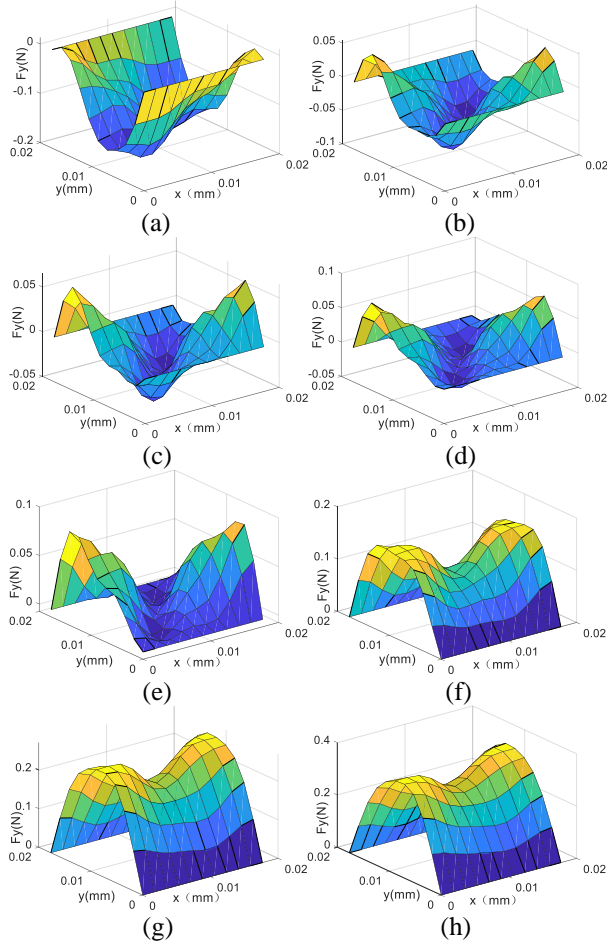
Fig. 11. The comparison of F_y with different fillet radius: (a) r=0, (b) r=0.5, (c) r=0.6, (d) r=0.7, (e) r=0.8, (f) r=1.2, (g) r=1.6, and (h) r=1.9.

Table 2: The max value of F_y with different fillet radius

r(mm)	Max value (N)	Ratio
0	0.1717	100%
0.5	0.0710	41.45%
0.6	0.0652	37.97%
0.7	0.0770	44.85%
0.8	0.0889	51.78%
1.2	0.1630	94.93%
1.6	0.2709	157.78%
1.9	0.3594	209.32%

Analyzing the value of Table 2 and the waveform of the Fig. 11, the F_y decreases firstly and then increases reversely with the fillet radius increase. The F_y can be reduced by optimizing the fillet radius of coil. For the planar motor of this paper, the F_y is significantly reduced when the fillet radius is equal to 0.6mm.

V. CONCLUSION

(1) The force integral expressions of corner segments of coil are given by Lorentz force law. The coil full model is used for calculating the force. The forces calculated by harmonic model, magnetic surface charge model and finite element model are compared, and the harmonic model is verified.

(2) The different coils can be obtained by changing the winding mould while keeping cl as constant. The forces of different coils are calculated by using the model verified before.

(3) The F_x decreases and the F_z increases with the fillet radius r increase. The F_y decreases firstly and then increases reversely as the fillet radius increase.

(4) The F_y caused by straight segments of coil is a small proportion. The F_y can be reduced by optimizing the fillet radius of coil. The F_y of short sides of coil is significantly reduced when the fillet radius takes 0.6. It has good theoretical and practical significance.

ACKNOWLEDGMENT

REFERENCES

[1] D. L. Trumper, M. E. Williams, and T. H. Nguyen, "Magnet arrays for synchronous machines," *Industry Applications Society Annual Meeting, 1993, Conference Record of the 1993 IEEE*, pp. 9-18, 1993.

[2] M. Lahdo, T. Ströhla, and S. Kovalev, "Magnetic propulsion force calculation of a 2-DoF large stroke actuator for high-precision magnetic levitation system," *Applied Computational Electromagnetics Society Journal*, vol. 32, no. 8, pp. 663-669, 2017.

[3] A. Nejadpak, M. R. Barzegaran, and O. A. Mohammed, "Evaluation of high frequency electro-magnetic behavior of planar inductor designs for resonant circuits in switching power converters," *Applied Computational Electromagnetics Society Journal*, vol. 26, no. 9, pp. 737-748, 2011.

[4] W.-J. Kim and D. L. Trumper, "High-precision magnetic levitation stage for photolithography," *Precision Engineering*, vol. 22, pp. 66-77, 1998.

[5] A. Shiri and A. Shoulaie, "Investigation of frequency effects on the performance of single-sided linear induction motor," *Applied Computational Electromagnetics Society Journal*, vol.

27, no. 6, pp. 497-504, 2012.

[6] K. Halbach, "Design of permanent multipole magnets with oriented rare earth cobalt materials," *Nuclear Instruments and Methods*, vol. 169, no. 6, pp. 1-10, 1980.

[7] J. C. Compter, "Electro-dynamic planar motor," *Precision Engineering*, vol. 28, pp. 171-180, 2004.

[8] J. W. Jansen, C. M. M. van Lierop, E. A. Lomonova, and A. J. A. Vandenput, "Modeling of magnetically levitated planar actuators with moving magnets," *IEEE Transactions on Magnetics*, vol. 43, no. 1, pp. 15-25, 2007.

[9] J. W. Jansen, C. M. M. van Lierop, E. A. Lomonova, and A. J. A. Vandenput, "Magnetically levitated planar actuator with moving magnets," *IEEE Transactions on Industry Applications*, vol. 44, no. 4, pp. 1108-1115, 2008.

[10] J. Peng, Y. Zhou, and G. Liu, "Calculation of a new real-time control model for the magnetically levitated ironless planar motor," *IEEE Transactions on Magnetics*, vol. 49, no. 4, pp. 1416-1422, 2013.

[11] Y. Zhou, G. Liu, R. Zhou, L. Huo, and W. Ming, "Modeling and comparison of the Halbach array with different segments per pole," *International Journal of Applied Electromagnetics and Mechanics*, vol.47, no. 3, pp. 629-641, 2015.

[12] G. Liu, Y. Zhou, R. Zhou, W. Ming, and L. Huo, "Analysis and optimization of a 2-D magnet array with hexagon magnet," *Applied Computational Electromagnetics Society Journal*, vol. 28, no. 10, pp. 976-983, 2013.

[13] G. Liu, Y. Wang, X. Xu, W. Ming, and X. Zhang, "The optimal design of real time control precision of planar motor," *Applied Computational Electromagnetics Society Journal*, vol. 32, no. 10, pp. 948-954, 2017.